Biosensors and Bioelectronics 177 (2021) 112968

Contents lists available at ScienceDirect

Biosensors and Bioelectronics

journal homepage: http://www.elsevier.com/locate/bios

Precise and rapid solvent-assisted geometric protein self-patterning with submicron spatial resolution for scalable fabrication of microelectronic biosensors

Jun'ya Tsutsumi [a,b,**], Anthony P.F. Turner [a,1], Wing Cheung Mak [a,*]

[a] Biosensors and Bioelectronics Centre, Division of Sensor and Actuator Systems, Department of Physics, Chemistry and Biology, Linköping University, SE-581 83, Linköping, Sweden

[b] Research Institute for Advanced Electronics and Photonics (RIAEP), National Institute of Advanced Industrial Science and Technology (AIST), 1-1-1 Higashi, Tsukuba, 305-8565, Japan

ARTICLE INFO

Keywords:
Protein micropatterning
Microelectronics
Bioelectrochemistry
Bioelectronics
Biointerfaces

ABSTRACT

Precise and high-resolution coupling of functional proteins with micro-transducers is critical for the manufacture of miniaturized bioelectronic devices. Moreover, electrochemistry on microelectrodes has had a major impact on electrochemical analysis and sensor technologies, since the small size of microelectrode affects the radial diffusion flux of the analyte to deliver enhanced mass transport and electrode kinetics. However, a large technology gap has existed between the process technology associated with such microelectronics and the conventional bio-conjugation techniques that are generally used. Here, we report on a high-resolution and rapid geometric protein self-patterning (GPS) method using solvent-assisted protein-micelle adsorption printing to couple biomolecules onto microelectrodes with a minimum feature size of 5 μm and a printing time of about a minute. The GPS method is versatile for micropatterning various biomolecules including enzymes, antibodies and avidin-biotinylated proteins, delivering good geometric alignment and preserving biological functionality. We further demonstrated that enzyme-coupled microelectrodes for glucose detection exhibited good electrochemical performance which benefited from the GPS method to maximize effective signal transduction at the bio-interface. These microelectrode arrays maintained fast convergent analyte diffusion displaying typical steady-state *I–V* characteristics, fast response times, good linear sensitivity (0.103 nA mm^{-2} mM^{-1}, $R^2 = 0.995$) and an ultra-wide linear dynamic range (2–100 mM). Our findings provide a new technical solution for the precise and accurate coupling of biomolecules to a microelectronic array with important implications for the scaleup and manufacture of diagnostics, biofuel cells and bioelectronic devices that could not be realized economically by other existing techniques.

1. Introduction

High resolution micropatterning of functional proteins is an essential tool in the design of many new diagnostic and therapeutic strategies. An essential prerequisite for widespread application is the ability to swiftly scale-up the procedure to make reproducible batches of devices or materials. Both high-throughput and point-of-care diagnostics demand improved manufacturing methods to meet increasingly diverse demands. Wearable and implantable biosensors are propitious examples which have attracted tremendous attention for real-time healthcare monitoring and maintenance of wellbeing (Koydemir and Ozcan, 2018). Microelectronics plays a key role in the development of such biosensors by facilitating the miniaturization necessary for *in vivo* sensing of biochemical responses in both tissues and intact organisms (Wightman, 2006; Lee et al., 2016; Meng et al., 2020). Moreover, a microelectrode with the dimension of tens of micrometers possesses a hemispherical or cylindrical diffusion flux of analyte with enhanced mass transport rates, which results in improved electrochemical kinetics and analytical

* Corresponding author.
** Corresponding author. Biosensors and Bioelectronics Centre, Division of Sensor and Actuator Systems, Department of Physics, Chemistry and Biology, Linköping University, SE-581 83, Linköping, Sweden.
E-mail addresses: junya.tsutsumi@aist.go.jp (J. Tsutsumi), wing.cheung.mak@liu.se (W.C. Mak).
[1] Current address: Professor Emeritus, SATM, Cranfield University, Cranfield, Bedford MK43 0AL, UK.

https://doi.org/10.1016/j.bios.2021.112968
Received 13 October 2020; Received in revised form 8 December 2020; Accepted 1 January 2021
Available online 8 January 2021

performance, such as faster response, higher sensitivity and wider dynamic range, compared with a macroelectrode where planar diffusion predominates (Matsui et al., 2017; Pemberton et al., 2011; Aoki et al., 1987; Kovach et al., 1985; Streeter et al., 2007; Ito et al., 1972; Compton et al., 2008). These superior characteristics are particularly important in wearable and implantable biosensors for real-time monitoring. In addition, an array of multiple microelectrodes (microelectrode array) is often used to overcome the low electric current associated with a single microelectrode (Li et al., 2019; Chen and White (2011); Hintsche et al., 1994).

Realizing the many advantageous properties of biomolecular arrays, however, is problematic due to the huge technology gap in process technology between microelectronics and conventional biomolecule immobilization techniques used in the manufacture of microelectronic biosensors. The most common practices of bulk-phase biomolecule immobilization onto microelectrodes using, for example, drop-casting of an enzyme sol-gel matrix (Llaudet et al., 2005, 2016) and glutaraldehyde crosslinking of the enzyme (Lourenco et al., 2016; Quinto et al., 2001), suffer from lack of precision and poor geometric alignment of biomolecules with the microelectrodes. In addition, the bulk immobilization matrix creates a planar diffusion layer that limits analyte diffusion and largely negates the advantages of using the microelectrode array. To develop high-performance microelectronic biosensors and diagnostics, it is important to immobilize the biomolecules precisely and specifically onto the microstructured transducer to maximize the bio-electrochemical signal transduction on the sensing surface.

Micropatterning of biomolecules has been achieved using various techniques such as photolithography, spotting (or inkjet printing), microcontact printing, and focused ion-beam (FIB) milling. Photolithography was established in the field of semiconductor processing and uses a patterned photoresist as a lift-off mask, which allows patterning of biomolecules with a submicron spatial resolution (Qiao et al., 2019; Blawas and Reichert, 1998). Spotting involves ejecting ink droplets from a nozzle onto a substrate, and therefore does not need masks or stamps and enables flexible patterning of biomolecules on demand (Kargl et al., 2015; Roth et al., 2004; Xu et al., 2005; Newman et al., 1992). Microcontact printing, a soft-lithography technique, uses a poly(dimethylsiloxane) (PDMS) stamp made by replicating a micro-structured silicon master fabricated by a semiconductor manufacturing process. In this method, the stamp is soaked with a biomolecule solution and is placed in conformal contact with a substrate surface to transfer a biomolecule layer from the stamp to the substrate surface (Nasseri et al., 2018; Kane et al., 1999; Bernard et al., 2000). FIB milling irradiates a focused ion beam to a pre-immobilized biomolecule layer to selectively remove the biomolecules at the irradiated position, which allows micropatterning of biomolecules with a few hundred nm spatial resolution (Jiang et al., 2008). Although these methods have been commonly used for biomolecule micropatterning, they need high precision alignment of a mask, a stamp, a nozzle, or an ion beam with a pre-patterned microelectrode array and multiple steps to immobilize biomolecules precisely aligned onto the microelectrode array; this severely hinders the development and scale-up of microelectronic biosensors. By contrast, wet/de-wet micropatterning, based on the spontaneous alignment of deposited materials guided by surface wettability of an underlying substrate, allows an alignment-free, high-throughput and scalable approach for biomolecule micropatterning. However, controlling the wet/de-wet behavior of biomolecules remains challenging due to their complex physio-chemical nature (Jachimska et al., 2016). For example, protein molecules consist of both hydrophobic and hydrophilic domains, causing water-soluble proteins to be strongly adsorbed on hydrophobic surfaces (Sethuraman et al., 2004).

Here we report a high resolution and rapid manufacturing method for microelectronic biosensors with a high-resolution and rapid geometric protein self-patterning (GPS) method for precise positioning and immobilization of proteins onto micro-transducers with a facile solvent-assisted wet/de-wet mechanism. With the GPS method, protein molecules were spontaneously aligned and patterned onto a microelectrode array with 5 μm spatial resolution. The microelectrode array was prepared by nanoparticle chemisorption printing which utilized an unique chemisorption effect of alkylamine-capped silver nanoparticles (AgNPs), enabling facile wet/dewet patterning of an ultrafine silver pattern with a minimum line width of 0.8 μm (Hirakawa et al., 2019; Aoshima et al., 2018; Kitahara et al., 2017; Yamada et al., 2016). The combination of the GPS method and the nanoparticle chemisorption printing enabled high-throughput manufacturing of microelectronic biosensors. We demonstrated the versatility of the GPS methods for high-resolution micro-patterning of various proteins including albumin, enzyme, antibody and avidin, and achieved excellent spatial alignment with the microelectrodes without significant loss of biomolecular activity. As a more detailed model, we chose the example of the extensively reported and characterized electrochemical glucose sensor (Newman and Turner, 2005; Sekretaryova et al., 2016) and manufactured microelectronic glucose biosensors by combining nanoparticle chemisorption printing, followed by rapid and high-resolution protein functionalization of the microelectrode via the GPS method, to produce sensors with superior electrochemical kinetics and analytical performance benefiting from the precise coupling of the bio-catalyst (i.e. enzyme) with the microelectrodes to maximize signal transduction and simultaneously to maintain the rapid convergent analyte diffusion characteristic originated from the microelectrode transducer.

2. Materials and methods

2.1. Materials

Perfluoropolymer, CYTOP CTL-809M, was purchased from Asahi Glass Co., Ltd., Japan. 50 wt% AgNP ink was synthesized by thermal decomposition of oxalate-bridging silver alkyl-amine complexes dispersed in 4:1 octane and butanol (Itoh et al., 2009). Bovine serum albumin, horseradish peroxidase (HRP), glucose oxidase from *Aspergillus niger* (GOx), biotinylation reagent, 3,3′,5,5′-tetramethylbenzidine (TMB) liquid substrate, and D-(+)-glucose were purchased from Sigma-Aldrich Co. LLC. Mouse immunoglobulin G (mouse IgG) and goat anti-mouse immunoglobulin G (anti-mouse IgG) were purchased from Arista biologicals Inc., USA. Streptavidin was purchased from Life technologies corporation, USA. Fluorescein-5-isothiocyanate (FITC) was purchased from Molecular probes, USA. Alexa fluor™ 594 NHS ester (Alexa) was purchased from Thermo Fisher Scientific Inc., USA.

2.2. Fluorescent protein labelling

FITC and Alexa were employed as fluorescent reagents. Dimethyl sulfoxide solution of the fluorescent reagent (50 μL) was added to a phosphate buffer solution of proteins (1 mL) with the molar ratio of reagent/protein = 3 and incubated for 8 h at 278 K in the dark. Then centrifugal filtration was performed to remove unreacted reagent, and the concentrate, fluorescently labelled protein, was dissolved into the desired solvents.

2.3. Biotinylation of HRP

Dimethyl sulfoxide solution of biotinylation reagent (30 μL) was added to phosphate buffer solution of HRP (1 mL) with the molar ratio of reagent/HRP = 13 and was incubated for 30 min at room temperature. Then centrifugal filtration was performed to remove unreacted reagent, and the concentrate, biotinylated HRP, was dissolved in the desired solvents.

2.4. Fabrication of silver (Ag) microelectrode arrays

Ag microelectrode arrays were fabricated by nanoparticle chemisorption printing (Yamada et al., 2016). Firstly, a perfluoropolymer

layer with a thickness of 700 nm (CYTOP CTL-809M) was spun-coated onto a glass substrate at 3000 rpm and then dried at 453 K for 30 min. The perfluoropolymer surface was then irradiated by vacuum ultraviolet light ($\lambda = 172$ nm) using a Xe_2 excimer lamp (VUS-3150, ORC manufacturing, Japan) through a photomask to prepare the patterned reactive surface [step 1 in Fig. 1(A)]. Finally, 50 wt% AgNP ink was blade-coated on the patterned reactive surface at 2 mm s^{-1} [step 2 in Fig. 1(A), Fig. S2 for more detail] and was annealed at 353 K for 30 min. The blade-coating of AgNP ink was conducted twice to obtain conductivity as high as 10^4 S cm^{-1} reproducibly, for the Ag microelectrode array.

2.5. Geometric protein self-patterning on Ag microelectrode array

Protein self-alignment on an Ag microelectrode array was examined for five kinds of proteins labelled by FITC; albumin, HRP, GOx, anti-mouse IgG, and streptavidin, with the tested solvents including acetic buffer solution (pH = 3.8, 4.8, 5.8; ionic strength = 15 mM), phosphate buffer solution (pH = 6.2, 7.2, 8.2; ionic strength = 15 mM), and acetone-buffer mixture 3:1 (v/v). For the preparation of acetone-buffer mixture solution for protein micropatterning, proteins were firstly dissolved in phosphate buffer solution (pH = 7.2; ionic strength = 15 mM), followed by addition of cooled acetone (at 253 K). The protein solutions were blade-coated on the Ag microelectrode array at 0.2 mm s^{-1} [step 3 in Fig. 1(A), Fig. S3 for more detail] and were dried at ambient temperature.

2.6. Catalytic activity test for self-patterned enzyme

The Ag microelectrode array immobilized with self-aligned FITC-conjugated HRP was fabricated by blade coating of 5 mg mL^{-1} HRP solution (acetone-buffer mixture; 3:1 v/v). Then it was immersed in 70 μM H_2O_2 containing TMB liquid substrate and was incubated at ambient temperature for 10 min. Subsequently, the blue color precipitate of oxidized TMB was examined using an optical microscope.

2.7. Affinity test for self-patterned antibody

The Ag microelectrode array on which FITC-conjugated anti-mouse IgG self-aligns was fabricated by blade coating of 20 mg mL^{-1} anti-mouse IgG solution (acetone-buffer mixture; 3:1 v/v). Then it was immersed in 20 mg mL^{-1} albumin solution (phosphate buffer solution;

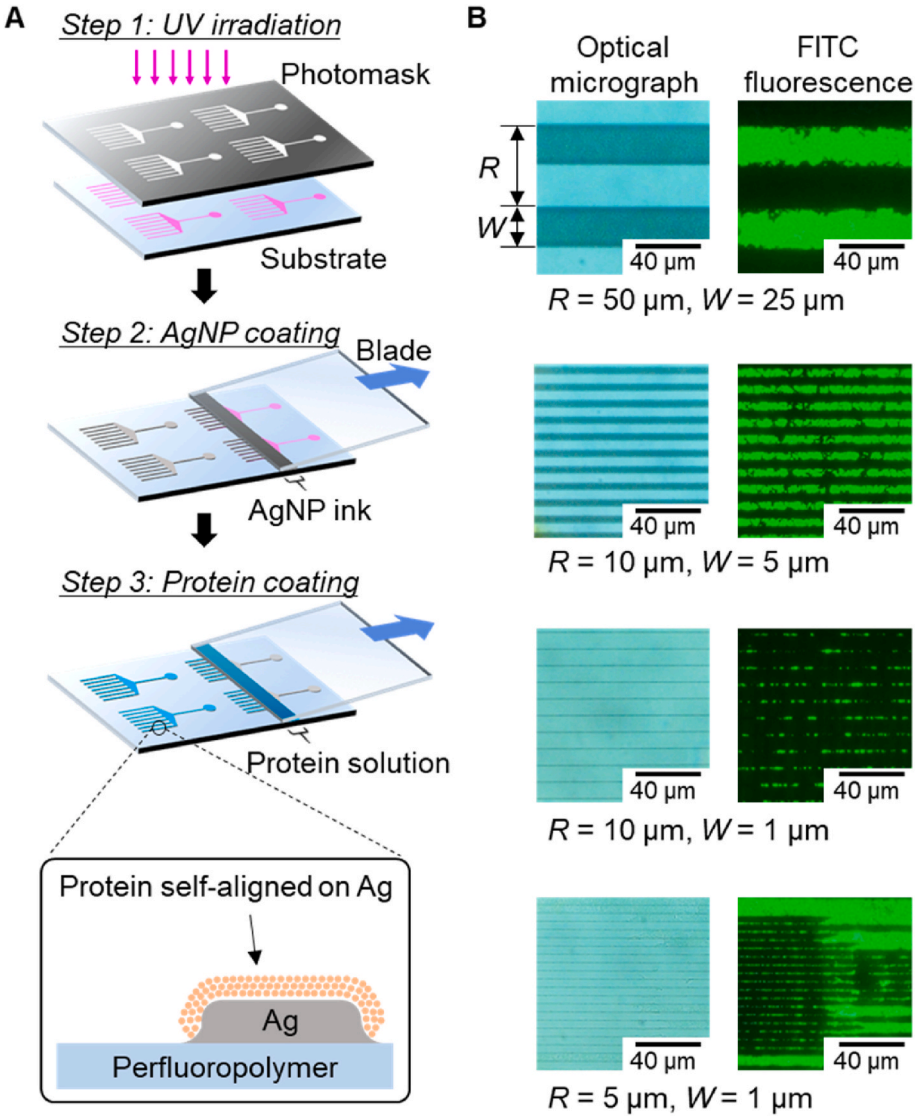

Fig. 1. Fabrication of Ag microelectrode arrays and protein self-patterning via blade coating. (A) High-resolution and rapid geometric protein self-patterning method via controlled surface wettability for scalable manufacturing of microelectronic biosensors. (B) Optical and fluorescence micrographs of the Ag microelectrode array with different repetition interval (R) and electrode width (W), which were coated by 5 mg mL^{-1} FITC-conjugated albumin solution.

pH = 7.2; ionic strength = 15 mM) for 1 h and was rinsed with water five times, which allowed an albumin blocking layer to form on the perfluoropolymer surface. The affinity test was carried out by immersing the Ag microelectrode array in 0.1 mg mL^{-1} Alexa-conjugated mouse IgG solution (phosphate buffer solution; pH = 7.2; ionic strength = 15 mM) for 2 h. Binding of mouse IgG to anti-mouse IgG was visualized using fluorescence microscopy where the FITC and Alexa were separately imaged by using two different optical bandpass filters.

2.8. Biotin binding test for self-patterned avidin

The Ag microelectrode array on which FITC-conjugated streptavidin self-aligns was fabricated by blade coating of 5 mg mL^{-1} streptavidin solution (acetone-buffer mixture; 3:1 v/v). Then it was immersed in 20 mg mL^{-1} albumin solution (phosphate buffer solution; pH = 7.2; ionic strength = 15 mM) for 1 h and was rinsed with water five times. The biotin binding test was conducted by immersing the Ag microelectrode array in 10 μg mL^{-1} biotinylated HRP solution (phosphate buffer solution; pH = 7.2; ionic strength = 15 mM) for 2 h. The resulting biotin binding was visualized by an HRP colorimetric assay where the Ag microelectrode array was immersed in 70 μM H_2O_2 containing TMB liquid substrate for 10 min.

2.9. Fabrication of microelectronic glucose biosensors

Microelectronic glucose biosensors were fabricated by a combination of nanoparticle chemisorption printing and the protein micro-patterning technique [Step 1–3 in Fig. 1(A)]. Firstly, a Ag microelectrode array (5 × 5 mm^2), composed of 500 microelectrodes (W = 5 μm, R = 10 μm; Fig. S1(A)), was fabricated as a working electrode platform by nanoparticle chemisorption printing. A few droplets of Ag nanoparticle ink (total volume = 6 μL) were applied onto a perfluoropolymer-coated glass substrate whose surface was photoactivated by vacuum ultraviolet light through a photomask, followed by printing of the Ag nanoparticle ink onto the glass substrate with a blade at a coating speed of 2 mm s^{-1}, controlled by a stepping motor (Fig. S2). Then GOx was immobilized onto the Ag microelectrode array by the protein micropatterning technique. An aliquot of 20 μL GOx solution (10 mg mL^{-1}) in an acetone-buffer mixture (3:1 v/v) was applied onto the Ag microelectrode, followed by printing of the GOx onto the Ag microelectrode with a blade at a coating speed of 0.2 mm s^{-1}, controlled by a motorized stage (Fig. S3).

2.10. Electrochemical measurements

Electrochemical measurements were performed using an electrochemical workstation (CompactStat, Ivium Technologies B.V., Netherlands) with a three-electrode system consisting of a Ag microelectrode array as the working electrode, a platinum wire as the counter electrode, and an Ag/AgCl electrode as the reference electrode. Measurements were carried out using 15 mM $LiClO_4$ electrolyte containing H_2O_2 or D-(+)-glucose. Amperometric measurement of H_2O_2 with the Ag microelectrode was performed by successively injecting aliquots of H_2O_2 and measuring at -0.05 V vs. Ag/AgCl under stirred condition. Amperometric measurement of glucose with the GOx immobilized Ag microelectrode was performed by applying 100 μL of glucose solution (2–100 mM) and measured at −0.05 V vs. Ag/AgCl under unstirred condition.

3. Results and discussion

3.1. Nanoparticle chemisorption printing of microelectrode array

Ag microelectrode arrays were fabricated by the nanoparticle chemisorption printing, as illustrated in Steps 1 and 2 of Fig. 1(A). A patterned photoactivated surface was prepared by irradiating a perfluoropolymer surface with vacuum-ultraviolet light and then exposed to AgNP ink by blade-coating. A thin solid silver layer eventually formed on the irradiated surface after a coating blade was swept across it, while the unirradiated surface remained bare (Figs. S1 and S2). The chemisorption printing process is fast that takes only ~6.75 s to create a fully patterned microelectrode array (i.e. a microelectrode array with a dimension of 13.5 × 5.0 mm with a blade-coating speed of 2 mm s^{-1}), while the process is possible to scale up with high-throughput parallel printing. Ag microelectrode arrays composed of high density and fine microband electrodes were obtained as shown in the optical micrographs of Fig. 1(B). The highest resolution obtained was an individual microband electrode width (W) of 1 μm with a repetition interval (R) of 5 μm, which is comparable to that obtained in our previous work (Yamada et al., 2016). Conductivity of the microelectrode as high as 6 × 10^4 S cm^{-1} was obtained after annealing at 353 K for 30 min.

3.2. GPS method for precise protein micropatterning on microelectrode arrays

The obtained microelectrode arrays were bio-functionalized by the GPS method via blade coating of protein solutions at a coating speed of 0.2 mm s^{-1} [step 3 in Fig. 1(A)]. The protein blade coating procedure takes ~1 min to create a well-aligned protein patterned onto a microelectrode array. Fig. 2(A) shows a fluorescence image of the microelectrode array after the deposition of FITC-conjugated albumin solution (phosphate buffer solution, pH 7.2). Fluorescence signal was observed over the entire substrate area, indicating that the albumin adsorbs on both the perfluoropolymer and Ag microelectrodes. Similar results were obtained over the solvent pH range of 5.8 to 8.2. In contrast, when the solvent pH was adjusted close to the isoelectric point (pI) of albumin (pH 3.8–4.8, pI albumin = 4.9), self-alignment of albumin on the Ag microelectrodes was observed [Fig. 2(B)]. It is generally known that proteins self-assemble into micelles at the pI since the intermolecular electrostatic repulsion is interrupted due to zero net charge of protein molecules (Shirahama and Suzawa, 1985). It is therefore postulated that the observed self-alignment is related to the self-assembly of protein molecules. To further investigate this hypothesis, we performed similar experiments by changing the solvent to acetone-buffer mixture, where acetone worked as a poor solvent to induce the protein self-assembly

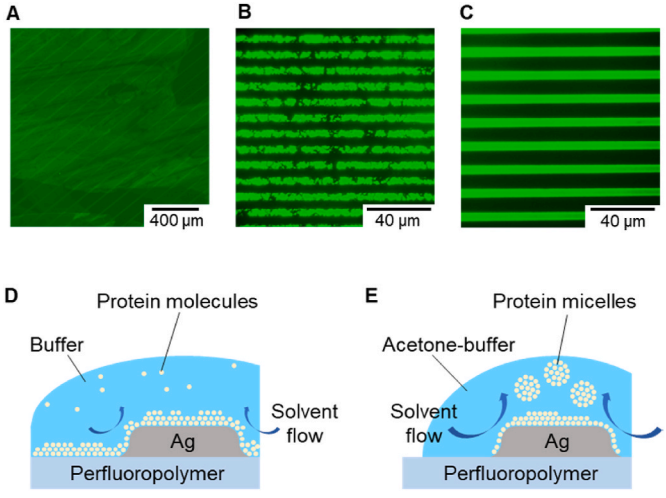

Fig. 2. Geometric protein self-patterning on an Ag microelectrode array. Fluorescence micrographs of the Ag microelectrode array coated by 5 mg mL^{-1} FITC-conjugated albumin with different solvents; (A) phosphate buffer solution (pH = 7.2), (B) phosphate buffer solution (pH3.8), and (C) acetone-buffer mixture (3:1 v/v). Schematic of (D) non-specific adsorption of protein 'molecules' in water and (E) specific adsorption of protein 'micelles' in acetone-buffer mixture.

(Myerson, 2002; Thorat and Dalvi, 2012). Fig. 2(C) shows the fluorescence image of the microelectrode array after deposition of FITC-conjugated albumin (acetone-buffer mixture; 3:1 v/v). As can be seen, self-alignment of albumin on the Ag microelectrode array was clearly observed, thus supporting our hypothesis. It is noteworthy that homogeneity of the self-aligned albumin was higher than that in the case where the pH value was adjusted.

Controlling the wet/de-wet behavior of proteins remains challenging due to their complex physio-chemical properties. Proteins consist of both hydrophobic and hydrophilic domains that cause non-selective adsorption onto both hydrophilic and hydrophobic surface. Even using a strongly hydrophobic perfluoropolymer surface with very low surface energy does not circumvent this problem unless the protein concentration is extremely low (<1 μg mL^{-1}) (Lee et al., 2003, 2004). The geometric protein self-patterning mechanism observed can be explained by considering the interface between the protein solution and the hydrophobic substrate of the microelectrode array. At the interface, a network of water hydrogen bonds is disrupted, which causes an increase of interfacial energy. To decrease the interfacial energy, 'amphiphilic' protein molecules spontaneously form the layer at the interface as shown in Fig. 2(D), which is a driving force for protein adsorption on a hydrophobic surface, i.e. the so-called hydrophobic interaction. In general, hydrophobic interaction is strengthened by protein self-assembly because it makes the proteins more insoluble (Wang and Christopher, 2010). This trend is apparently contradicted by the result obtained in this work. In this regard, however, we should consider the fact that the hydrophobic interaction works only in an aqueous environment. In the blade coating process, a substrate surface is exposed to the air immediately after sweeping the blade [step 3 in Fig. 1(A)], which is much different from conventional protein deposition involving relatively long incubation times, such as drop-casting. Therefore, weak van der Waals force dominates as the adsorption force of proteins onto a hydrophobic substrate surface. Since the van der Waals force is a short-range force whose energy is one order smaller than that of the hydrophobic interaction (Israelachvili, 1992), sparse contact of protein micelles may cause easier desorption from the hydrophobic surface than close contact of protein molecules [Fig. 2(D)(E)]. The desorbed protein micelles would be transported by the solvent flow generated in the blade coating process. At the substrate region where the blade passes through, the solvent rapidly shrinks onto the hydrophilic microelectrodes away from the hydrophobic perfluoropolymer surface. Solvent flow generated by this shrink drives protein micelles from the hydrophobic region to the hydrophilic region [Fig. 2(E)]. Acetone-buffer mixture may have the effect of enhancing the solvent flow due to its fast evaporation, as associated with the homogeneous self-alignment observed [Fig. 2(C)].

The spatial resolution of the GPS technique was examined by systematically changing the repetition interval (R) and the electrode width (W) of the microelectrode array. Fig. 1(B) shows the results for the albumin solution. As can be seen in the fluorescence micrographs, line collapse was observed at $R \leq 5$ μm, and a decrease of protein coverage on the microelectrodes was observed at $W \leq 1$ μm. From these results, the maximum resolution was estimated at $R = 10$ μm and $W = 5$ μm. The immobilization stability of proteins self-aligned on a microelectrode array was examined by monitoring fluorescence decay resulting from desorption of the FITC-conjugated albumin upon immersion in Milli-Q water. Fig. 3 shows fluorescence images taken at different time intervals. As can be seen, the fluorescence intensity decreases after immersing the microelectrode array in Milli-Q water, retaining 95.1% and 88.6% of the fluorescence intensity after 0.2 h and 2 h incubation, respectively. The decreases in fluorescence intensity likely results from protein desorption or decay of the fluorescence label. As discussed above, geometric protein self-patterning can be realized under two different conditions, i.e. adjusting solvent pH to the protein pI or using a poor solvent. However, proteins with different pI require fine tuning of solvent pH depending on the physiochemical nature of the protein materials. In contrast, micropatterning using the acetone-buffer mixture

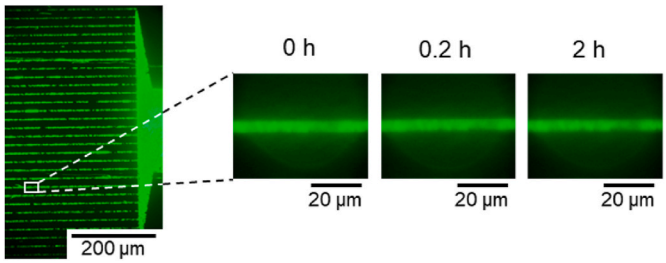

Fig. 3. Protein immobilization stability onto an Ag microelectrode array. Fluorescence micrographs of FITC-conjugated albumin self-aligned on an Ag microelectrode array following immersion in Milli-Q water. The micrographs were taken at 0 h, 0.2 h and 2 h after immersing in water.

can be universally applied for various proteins without any additional procedures. Therefore, the acetone-buffer method was chosen for further studies on micropatterning of enzymes, antibodies, and streptavidin onto microelectrodes.

3.3. Versatility of the GPS method for protein micropatterning

The versatility of the GPS technique was examined for various proteins. Fig. 4(A)(C)(E) show the results for self-patterning of HRP (enzyme), anti-mouse IgG (antibodies), and streptavidin (tetrameric biotin-binding protein) with acetone-buffer mixture as the solvent. For all the cases, it was clearly observed that the fluorescence signal of the FITC-conjugated proteins was well-aligned with the Ag microelectrode array, indicating that the GPS technique is universally applicable to these proteins. The applicability to streptavidin is particularly important because it allows the introduction of various biotinylated biomolecules through avidin-biotin binding. This feature widens the applications of this technique for the fabrication of various affinity biosensors and immunodiagnostic devices.

We further examined the influence of the GPS process on the biofunctionalities of proteins. The catalytic activity of the enzyme, HRP, was routinely visualized using a TMB substrate, which yielded a characteristic blue-colored enzymatic product as a result of the reaction catalyzed by HRP. Fig. 4(A) shows the self-patterned HRP on microelectrodes and Fig. 4(B) shows the result of the corresponding colorimetric assay. It was clearly observed that the footprint of the blue colored enzymatic product was well aligned with the HRP-functionalized microelectrodes, indicating that the self-patterned HRP preserves its catalytic activity. More importantly, the localization of the enzymatic product at the microelectrodes maximized the signal transduction at the transducer interface.

The affinity function of the antibody, anti-mouse IgG, was examined by immunoassay using mouse IgG. Fig. 4(C) shows the self-patterned anti-mouse IgG onto the microelectrodes, and Fig. 4(D) shows the result of the corresponding fluorescence affinity immunoassay. It was observed that the fluorescence image of Alexa-conjugated mouse IgG coincided well with that of FITC-conjugated anti-mouse IgG. The result indicates that the self-patterned anti-mouse IgG preserves its specific affinity with respect to mouse IgG. Moreover, it is significantly important for affinity biosensing to obtain a good geometric alignment of the capture antibodies onto transducer, in order to ensure the binding of the antigen and formation of the immunocomplex is localized solely at the microelectrode region to maximize the signal transduction.

The biotin binding capability of streptavidin was examined by affinity capture of biotinylated-HRP, followed by colorimetric assay to visualize the biotinylated-HRP captured by streptavidin. Fig. 4(E) shows the self-patterned streptavidin on the microelectrodes, and Fig. 4(F)(G) show the result of the corresponding affinity captured biotinylated-HRP. By comparing the optical images taken before [Fig. 4(F)] and after the HRP catalyzed colorimetric assay [Fig. 4(G)], it was shown that the blue colored precipitate of oxidized TMB, resulting from the catalytic

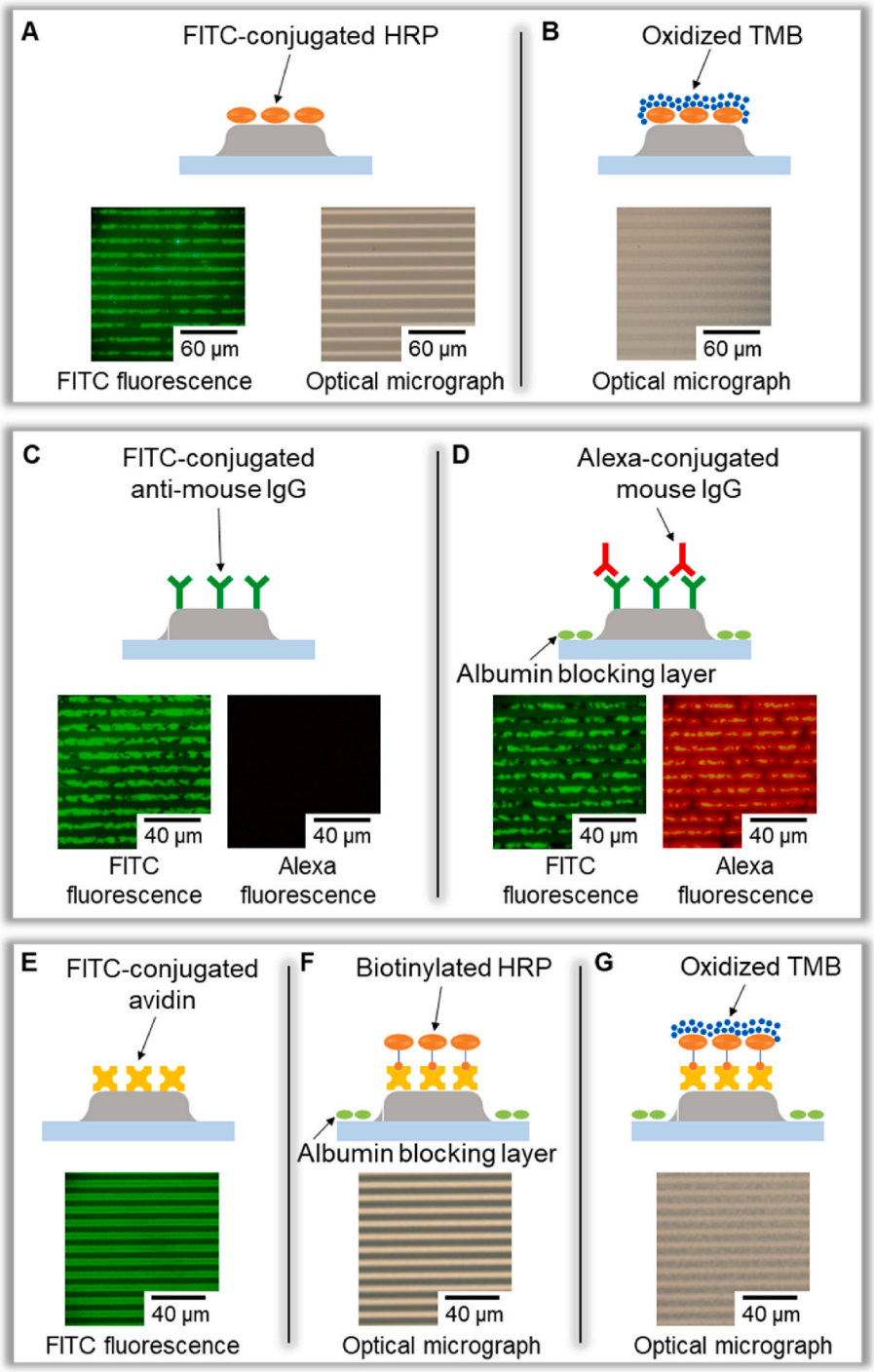

Fig. 4. The versatility of GPS method for precise protein micro-patterning. Schematic, fluorescence micrograph, and optical micrographs of FITC-conjugated HRP self-aligned on a Ag microelectrode array (A) before and (B) after colorimetric assay. Schematic and fluorescence micrograph of FITC-conjugated anti-mouse IgG self-aligned on a Ag microelectrode array (C) before and (D) after affinity assay using Alexa-conjugated mouse IgG. Schematic, fluorescence and optical micrograph of FITC-conjugated avidin self-aligned on a Ag microelectrode array (E) before avidin-biotin complex formation, (F) after avidin-biotin complex formation, and (G) after colorimetric assay.

reaction of HRP, was well aligned with the microelectrodes pattern. The results indicate that the biotin binding capability of self-aligned streptavidin is preserved, as well as the catalytic activity of the biotinylated-HRP introduced by the biotin-avidin binding precisely onto the microelectrode array.

3.4. Fabrication of microelectronic glucose biosensors

To demonstrate the GPS technique for manufacturing bioelectronic devices and performing bioelectrochemistry on microelectrodes, a microelectronic glucose biosensor was fabricated by the nanoparticle chemisorption printing of an Ag microelectrode array [step 1,2 in Fig. 1(A)] followed by self-patterning of GOx onto the microelectrodes [step 3 in Fig. 1(A)]. Fig. 5(A)(B) shows optical and fluorescence micrographs taken of the microelectronic glucose biosensor where GOx self-patterned and well-aligned on the microelectrode array ($W = 5$ μm, $R = 10$ μm). The fluorescence intensity is uniform over most of the area of the microelectrodes, although small fluctuations are found in several spots [Fig. 5(C)]. These spots were also observed in SEM and AFM images [Fig. 5(E)(G)], and their size estimated from the AFM height profile [Fig. 5(H)] was about 100 nm, which was much larger than the size of the GOx molecule (6 nm) (Libertino et al., 2008; Wilson and Turner, 1992). Except for these spots, the height profile over most of the area of the microelectrodes was quite uniform. The thickness of the GOx layer in

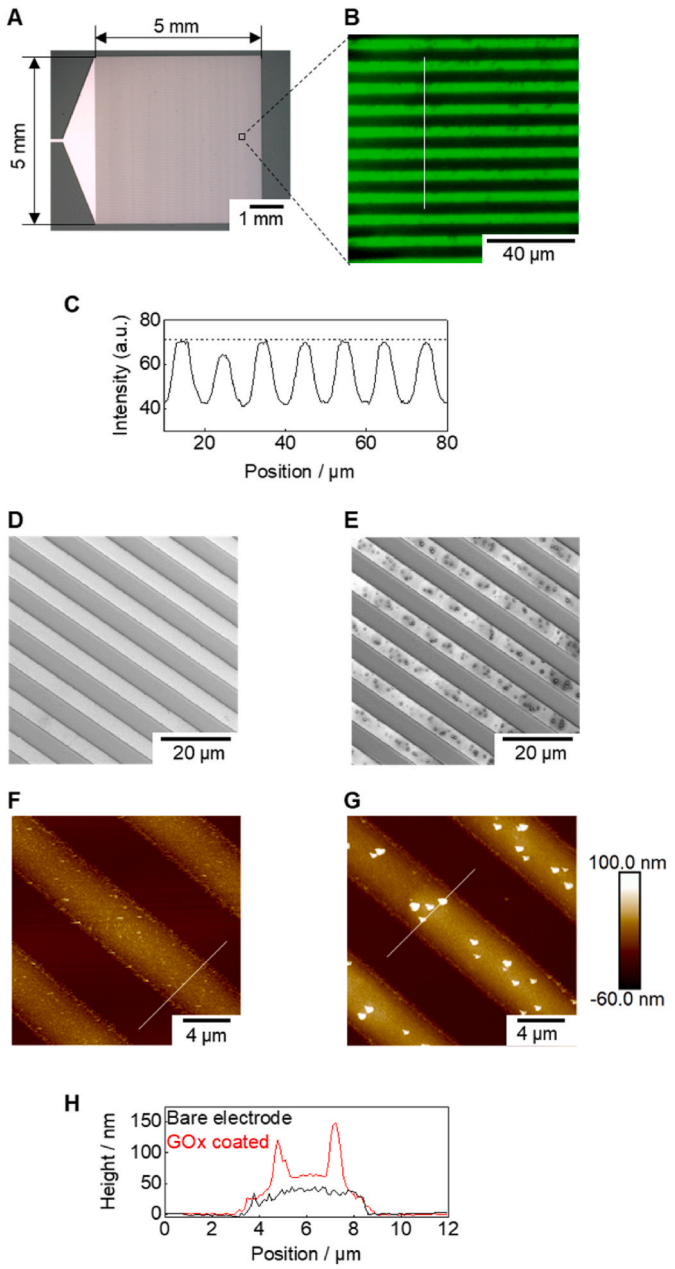

Fig. 5. Surface characterization of the microelectronic glucose biosensor. (A) Optical and (B) fluorescence micrographs of the Ag microelectrode array on which FITC-conjugated GOx self-aligns. (C) Intensity profile along the white line shown in (B). SEM images of the Ag microelectrode array (D) without and (E) with self-aligned GOx. AFM images of the Ag microelectrode array (F) without and (G) with self-aligned GOx. (H) Height profiles along the white lines shown in (F) and (G).

the uniform area was estimated to be 20 nm (~3 molecular layers) from the comparison of the height profiles between the GOx-coated and bare microelectrodes [Fig. 5(H)]. These results imply that the GOx micelles reassemble into a fairly uniform film structure when they adsorb onto the microelectrodes. The highest spots are most probably due to excess GOx micelles adsorbing onto the uniform GOx layer.

The glucose sensing capability of the fabricated microelectronic glucose biosensor was examined, to show proof-of-principle, according to the following catalytic reaction:

$$\text{Glucose} + O_2 + 2H_2O \xrightarrow{GOX} \text{Gluconic acid} + 2H_2O_2$$

The glucose concentration is proportional to the product of the above reaction, H_2O_2, which can be detected by the Ag microelectrode array through the electrocatalytic activity of Ag toward electro-reduction of H_2O_2 (Wen et al., 2013). To confirm this, we firstly measured cyclic voltammograms and amperometric responses of H_2O_2 by using the printed Ag microelectrode array as the working electrode. As shown in Fig. 6(A), the result measured for 1.5 mM H_2O_2 shows a typical steady-state *I–V* characteristic featured by a constant current at the voltage range between −0.2 and 0.0 V, which originates from convergent analyte diffusion with enhanced mass transport (Bond et al., 1988). Control experiments performed by the addition of 100 mM glucose to the bare Ag microelectrode array did not show any significant response [Fig. 6(A)]. Amperometric responses toward successive injections of H_2O_2 exhibited good linearity and sensitivity (0.569 nA mm^{-2} mM^{-1}, R^2 0.997) [Fig. 6(B)].

We further examined the performance of the microelectronic glucose biosensor composed of the printed Ag microelectrode array with self-patterned GOx. As seen in Fig. 6(C), the cyclic voltammogram obtained by the microelectronic glucose sensor in response to 100 mM glucose retained steady-state *I–V* characteristics of the microelectrodes after functionalization with GOx by the GPS method. Fig. 6(D)(E) shows amperometric responses to 2–10 mM and 20–100 mM glucose, respectively. The current plotted was measured immediately after applying a voltage of −0.05 V vs. Ag/AgCl, so that the observed current decay originates from a decrease of the H_2O_2 concentration at the electrode interface resulting from electro-reduction. In Fig. 6(F), the current responses measured at different time intervals [20,40, 60 s in Fig. 6(D)(E)] were plotted as a function of glucose concentration. As can be seen, a linear relationship was obtained for the range of 2–20 mM, 2–60 mM and 2–100 mM, for the measurements taken at 20, 40, and 60 s with sensitivity of 0.178, 0.120 and 0.103 nA mm^{-2} mM^{-1} and corresponding R^2 of 0.999, 0.997 and 0.995, respectively. Moreover, the microelectronic glucose biosensors exhibited an ultra-wide linear range between 2 to 100 mM. Such wide-range linearity and rapid current response are likely benefits from the precise immobilization of GOx onto the microelectrodes that retain convergent analyte diffusion, with the consequent enhanced diffusion of glucose analyte at the microelectrode interface.

We further compared the GPS immobilization of GOx onto a microelectrode with a conventional bulk drop-cast immobilization with chitosan for the preparation of the glucose biosensors and compared the analytical performance. The drop-cast GOx immobilization was performed by dropping 10 μL of GOx solution (10 mg mL^{-1}) onto the microelectrode, covered with a glass slide and incubated for 30 min. Then, 2 μL of chitosan solution (0.1%) was dropped onto the GOx electrode as the encapsulation layer and allows drying for 1 h at 4 °C (Zhang et al., 2014). The amperometric response of the drop-casted chitosan/GOx biosensor for the detection of 2–100 mM glucose was shown in the Fig. S4(A) and the corresponding calibration curve measured at 50s was shown in Fig. S4(B). The current response of the drop-casted chitosan/GOx biosensor was lower (~2.14 times lower) compared with the GPS immobilized GOx biosensor (Fig. 6(D-E)), likely caused by the chitosan matrix that affects the glucose response. Moreover, the drop-casted chitosan/GOx biosensor had a narrow linear range from 2-10 mM (compared with 2–100 mM for the GPS GOx biosensor) which is likely due to a diffusion limitation from the chitosan/enzyme matrix that hindered the rapid analyte diffusion properties of the microelectrode (Compton et al., 2008). Interestingly, we further compared the literature reports of microelectrode-based glucose biosensors prepared by conventional drop-cast enzyme immobilization and found that they show narrow linear ranges only up to about 10 mM glucose or as low as 2 mM glucose (Hughes et al., 2018; Ju et al., 1998; Pemberton et al., 2009; Pemberton et al. 2009a; Pemberton et al. 2011). This result indicates the GPS method facilitates the diffusion kinetics of microelectrode for biosensing with an ultra-wide linear range. The main focus of this work is on precise geometric protein patterning with a submicron spatial resolution for the immobilization of biomolecules

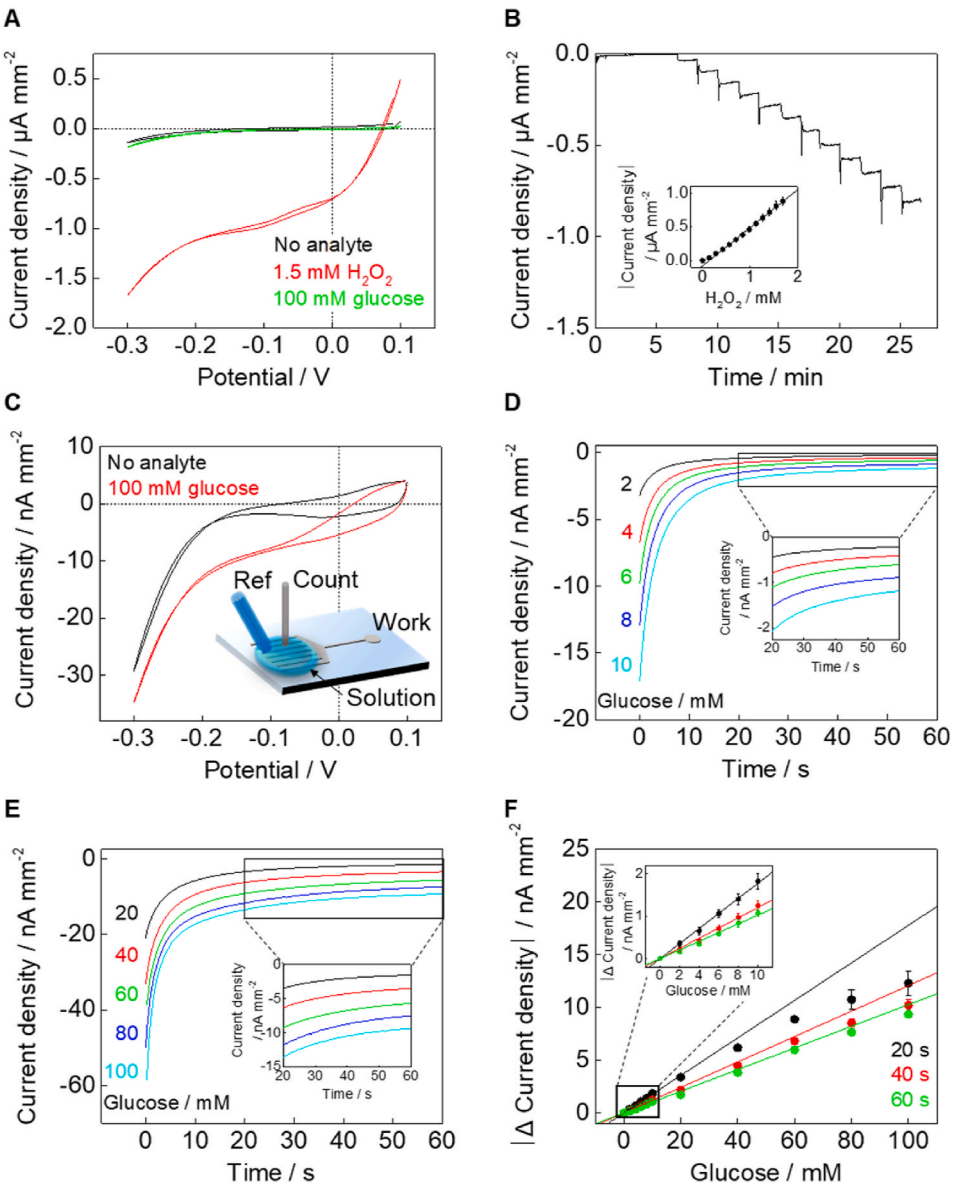

Fig. 6. (A) Cyclic voltammograms for no analyte, 1.5 mM H_2O_2, and 100 mM glucose measured by using a bare Ag microelectrode array as the working electrode. (B) Amperometric response (stirred) of the bare Ag microelectrode array toward successive injection of aliquots of H_2O_2 at −0.05 V vs. Ag/AgCl. Each current step corresponds to 0.14 mM increase of H_2O_2 concentration. The inset shows the current response vs. H_2O_2 concentration. (C) Cyclic voltammograms for no analyte and 100 mM glucose measured by using the Ag microelectrode array with self-aligned GOx as the working electrode. The measurements were conducted by casting the 100 μL sample solution on the Ag microband electrode as shown in the inset. And amperometric response (unstirred) of the Ag microelectrode array with self-aligned GOx toward casting 100 μL sample solution at −0.05 V vs. Ag/AgCl; (D) 2–10 mM and (E) 20–100 mM glucose. (F) Current response vs. glucose concentration at 20, 40 and 60 s.

onto micro-scale transducer. The overall sensitivity of the biosensors is determined by the electrode materials and requires further investigation.

The proof-of-concept microelectronic glucose biosensor fabricated in this work is based on electrochemical detection of enzymatically generated H_2O_2 by glucose oxidase (also known as the 1st generation non-mediated biosensor). For this configuration, we suffered a similar limitation on interferences caused by other redox-active substances. However, the main focus of this work is on the precise and rapid geometric self-patterning of protein with a submicron spatial resolution for the immobilization of biomolecules onto micro-scale transducer, and we demonstrated this by the fabrication of a microelectronic glucose biosensor using the GPS method. In future, it would be possible to introduce mediators or inorganic catalysts (e.g. Prussian blue) to minimize the effect from interferences for catalytic biosensors (Deng et al., 2014; Ricci and Palleschi, 2005). Moreover, it is important to note that the GPS immobilization method is versatile for micropatterning various biomolecules including enzymes, antibodies and other avidin-biotinylated proteins as demonstrated. Thus, the method could potentially be applicable broadly to other non-catalytic electrochemical biosensors (e.g. acoustic or impedimetric biosensors), as well as optical biosensors and microarrays.

4. Conclusion

In summary, we demonstrate a rapid and high-resolution GPS method for effective immobilization of protein molecules onto a microelectrode array supported by a hydrophobic perfluoropolymer surface for the fabrication of microelectronic biosensors. This GPS technique enabled high-resolution protein micropatterning applicable to various proteins such as albumin, enzyme, antibody, and avidin, without loss of their bio-functionalities. By combining it with nanoparticle chemisorption printing, which allowed high-throughput wet/dewet patterning of microelectrode arrays by the unique chemisorption effect of AgNPs, the GPS technique enabled a facile fabrication of a microelectronic glucose sensor with good sensitivity, fast response and surprisingly wide-range linearity. This proof-of-principle demonstrated a general approach that could be the key to realizing the on-demand mass production of bioelectronics to satisfy the growing demand for an “Internet of things (IoT)” sensor market as well as providing a generally scalable approach for biomolecular patterning and the fabrication of bioelectronic devices such as fuel cells and biocomputers.

CRediT authorship contribution statement

Jun'ya Tsutsumi: Conceptualization, Data curation, Formal analysis, Investigation, Writing - original draft. **Anthony P.F. Turner:** Formal analysis, Investigation, Writing - review & editing, Supervision. **Wing Cheung Mak:** Conceptualization, Formal analysis, Investigation, Writing - review & editing, Supervision.

Declaration of competing interest

The authors declare that they have no known competing financial interests or personal relationships that could have appeared to influence the work reported in this paper.

Acknowledgement

The author would like to acknowledge the financial support by the JSPS KAKENHI grant number JP19H02587, and the Swedish Research Council grant number VR-2015-04434. We are grateful to Mr. Gyo Kitahara and Prof. Tatsuo Hasegawa (Department of Applied Physics, The University of Tokyo) for their help in the nanoparticle chemisorption printing of Ag microelectrode arrays.

Appendix A. Supplementary data

Supplementary data to this article can be found online at https://doi.org/10.1016/j.bios.2021.112968.

References

Aoki, K., Tokuda, K., Matsuda, H., 1987. J. Electroanal. Chem. 225, 19–32.
Aoshima, K., Hirakawa, Y., Togashi, T., Kurihara, M., Arai, S., Hasegawa, T., 2018. Sci. Rep. 8, 6133.
Bernard, A., Renault, J.P., Michel, B., Bosshard, H.R., Delamarche, E., 2000. Adv. Mater. 12, 1067–1070.
Blawas, A.S., Reichert, W.M., 1998. Biomaterials 19, pp. 595–609.
Bond, A.M., Oldham, K.B., Zoski, C.G., 1988. J. Electroanal. Chem. Interfacial Electrochem. 245, 71–104.
Chen, I.-J., White, I.M., 2011. Biosens. Bioelectron. 26, 4375.
Compton, R.G., Wildgoose, G.G., Rees, N.V., Streeter, I., Baron, R., 2008. Chem. Phys. Lett. 459, 1–17.
Deng, H., Teo, A.K.L., Gao, Z., 2014. Sensor. Actuator. B Chem. 191, 522–528.
Hintsche, R., Paeschke, M., Wollenberger, U., Schnakenberg, U., Wagner, B., Lisec, T., 1994. Biosens. Bioelectron. 9, 697–705.
Hirakawa, Y., Aoshima, K., Arai, S., Hasegawa, T., 2019. ACS Appl. Nano Mater. 2, 4342–4349.
Hughes, G., Pemberton, R.M., Nicholas, P., Hart, J.P., 2018. Electroanalysis 30, 1616–1620.
Israelachvili, J., 1992. Intermolecular and Surface Forces. Academic press ltd., London.
Ito, C.R., Asakura, S., Nobe, K., 1972. J. Electrochem. Soc. 119, 698–701.
Itoh, M., Kakuta, T., Nagaoka, M., Koyama, Y., Sakamoto, M., Kawasaki, S., Umeda, N., Kurihara, M., 2009. J. Nanosci. Nanotechnol. 9, 6655–6660.
Jachimska, B., Tokarczyk, K., Łapczyńska, M., Puciul-Malinowska, A., Zapotoczny, S., 2016. Colloids Surf. A Physicochem. Eng. Asp. 489, 163–172.
Ju, H., Zhou, D., Xiao, Y., Chen, H., 1998. Electroanalysis 10, 541–545.
Jiang, J., Li, X.M., Mak, W.C., Trau, D., 2008. Adv. Mater. 20, 1636–1643.
Kane, R.S., Takayama, S., Ostuni, E., Ingber, D.E., Whitesides, G.M., 1999. Biomaterials 20, pp. 2363–2376.
Kargl, R., Vorraber, V., Ribitsch, V., Köstler, S., Stana-Kleinschek, K., Mohan, T., 2015. Biosens. Bioelectron. 68, 437–441.
Kitahara, G., Aoshima, K., Tsutsumi, J., Minemawari, H., Arai, S., Hasegawa, T., 2017. Org. Electron. 50, 426–428.
Kovach, P.M., Caudill, W.L., Peters, D.G., Wightman, R.M., 1985. J. Electroanal. Chem. 185, 285–295.
Koydemir, H.C., Ozcan, A., 2018. Annu. Rev. Anal. Chem. 11, 127–146.
Lee, C.S., Lee, S.H., Park, S.S., Kim, Y.K., Kim, B.G., 2003. Biosens. Bioelectron. 18, 437–444.
Lee, J.H., Kim, H., Kim, J.H., Lee, S.H., 2016. Lab Chip 16, 959–976.
Lee, S.H., Lee, C.S., Shin, D.S., Kim, B.G., Lee, Y.S., Kim, Y.K., 2004. Sensor. Actuator. B Chem. 99, 623–632.
Libertino, S., Aiello, V., Scandurra, A., Renis, M., Sinatra, F., 2008. Sensors 8, 5637–5648.
Li, D., Batchelor-McAuley, C., Chen, L., Compton, R.G., 2019. ACS Sens. 4, 2250–2266.
Llaudet, E.C., Darimont, D., Samba, R., Matiychyn, I., Stelzle, M., Weissenborn, M.J., Hauer, B., 2016. Chembiochem 17, 1367–1373.
Llaudet, E., Hatz, S., Droniou, M., Dale, N., 2005. Anal. Chem. 77, 3267–3273.
Lourenco, C.F., Ledo, A., Laranjinha, J., Gerhardt, G.A., Barbosa, R.M., 2016. Sensor. Actuator. B Chem. 237, 298–307.
Matsui, Y., Hamamoto, K., Kitazumi, Y., Shirai, O., Kano, K., 2017. Anal. Sci. 33, 845–851.
Meng, L., Turner, A.P.F., Mak, W.C., 2020. Biotechnol. Adv. 39, 107398.
Myerson, A.S. (Ed.), 2002. Handbook of Industrial Crystallization. Butterworth-Heinemann, Massachusetts.
Nasseri, B., Soleimani, N., Rabiee, N., Kalbasi, A., Karimi, M., Hamblin, M.R., 2018. Biosens. Bioelectron. 117, 112–128.
Newman, J.D., Turner, A.P.F., 2005. Biosens. Bioelectron. 20, 2435–2453.
Newman, J.D., Turner, A.P.F., Marrazza, G., 1992. Anal. Chim. Acta 262, 13–17.
Pemberton, R.M., Xu, J., Pittson, R., Drago, G.A., Griffiths, J., Jackson, S.K., Hart, J.P., 2011. Biosens. Bioelectron. 26, 2448–2453.
Pemberton, R.M., Pittson, R., Biddle, N., Hart, J.P., 2009. Biosens. Bioelectron. 24, 1246–1252.
Pemberton, R.M., Xu, J., Pittson, R., Biddle, N., Drago, G.A., Jackson, S.K., Hart, J.P., 2009a. Anal. Biochem. 385, 334–341.
Qiao, F., Guo, Q., Tu, Q., Lu, J., Wang, J., Tian, W., Xiong, K., Huang, N., Yang, Z., 2019. Langmuir 35, 7175–7179.
Quinto, M., Koudelka-Hep, M., Palmisano, F., 2001. Analyst 126, 1068–1072.
Roth, E.A., Xu, T., Das, M., Gregory, C., Hickman, J.J., Boland, T., 2004. Biomaterials 25, 3707–3715.
Ricci, F., Palleschi, G., 2005. Biosens. Bioelectron. 21, 389–407.
Sekretaryova, A.N., Eriksson, M., Turner, A.P.F., 2016. Biotechnol. Adv. 34, 177–197.
Sethuraman, A., Han, M., Kane, R.S., Belfort, G., 2004. Langmuir 20, 7779–7788.
Shirahama, H., Suzawa, T., 1985. Colloid Polym. Sci. 263, 141–146.
Streeter, I., Fietkau, N., Del Campo, J., Mas, R., Munoz, F.X., Compton, R.G., 2007. J. Phys. Chem. C 111, 12058–12066.
Thorat, A.A., Dalvi, S.V., 2012. Chem. Eng. J. 181, 1–34.
Wang, W., Christopher, R. (Eds.), 2010. Aggregation of Therapeutic Proteins. John Wiley & Sons, Inc., New Jersey.
Wen, Y., Lin, A.J., Chen, H.F., Jiao, Y.Z., Yang, H.F., 2013. Biosens. Bioelectron. 41, 857–861.
Wightman, R.M., 2006. Science 311, 1570–1574.
Wilson, R., Turner, A.P.F., 1992. Biosens. Bioelectron. 7, 165–185.
Xu, T., Jin, J., Gregory, C., Hickman, J.J., Boland, T., 2005. Biomaterials 26, 93–99.
Yamada, T., Fukuhara, K., Matsuoka, K., Minemawari, H., Tsutsumi, J., Fukuda, N., Aoshima, K., Arai, S., Makita, Y., Kubo, H., Enomoto, T., Togashi, T., Kurihara, M., Hasegawa, T., 2016. Nat. Commun. 7, 11402.
Zhang, Y., Li, Y., Wu, W., Jiang, Y., Hu, B., 2014. Biosens. Bioelectron. 60, 271–276.